# Germanium Growth Orientation on SrTiO3 (001) 2× 1 Surface: Role of Surface Reduction

**ARTICLE** *in* THE JOURNAL OF PHYSICAL CHEMISTRY C · APRIL 2013

Impact Factor: 4.77 · DOI: 10.1021/jp4013976



**2 AUTHORS:**

Junjie Wang
National Institute for Materials Science
**17** PUBLICATIONS **152** CITATIONS
SEE PROFILE

Isabelle Lefebvre
Institut Supérieur de l'Electronique et du Num…
**42** PUBLICATIONS **622** CITATIONS
SEE PROFILE

THE JOURNAL OF PHYSICAL CHEMISTRY C

Article

pubs.acs.org/JPCC

# Germanium Growth Orientation on $SrTiO_3$ (001) 2 × 1 Surface: Role of Surface Reduction

Junjie Wang[†] and Isabelle Lefebvre*[,†]

[†]IEMN, Departement ISEN (UMR 8520 CNRS), 41 boulevard Vauban, 59046 Lille Cedex, France

**ABSTRACT:** We present a theoretical study of germanium growth orientation dependence on $SrTiO_3$ surface structure using first-principles calculations. Contrary to much work on the $SrTiO_3$ surface which considers the simple $TiO_2$ termination, we work on the now well known 2 × 1 reconstructed surface, which is terminated with a $TiO_2$ double layer.[29] We study the oxygen reduction at this surface maintaining the 2 × 1 reconstruction. Analysis of its electronic structure shows that the reduction leads to a metallic surface and changes of the surface bond characteristics. Therefore, the growth routes for Ge epitaxy are studied. It is demonstrated that the reduction favors the creation of the Ge−O bonds by weakening the strength of the Ti−O bonds. It gives the possibility of Ge[001] growth direction, which is not possible on a nonreduced surface.

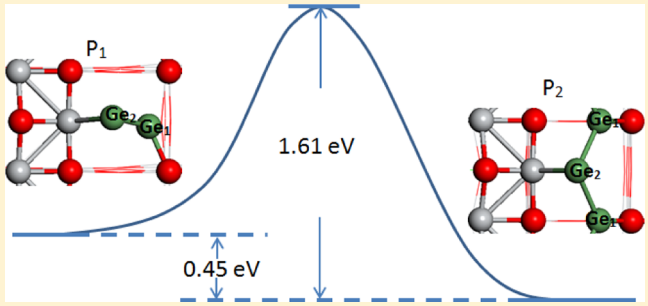


## 1. INTRODUCTION

III−V and Ge-based semiconductors, with their high carrier mobility and excellent optoelectronic functionalities, are considered as potential candidates for a channel material in forthcoming complementary metal-oxide semiconductor (CMOS) devices.[1−3] To grow epitaxial films of these materials on silicon gives a very promising route to integrate micro- and optoelectronic functionalities on the same wafer. However, the direct heteroepitaxial growth of III−V or Ge-based semiconductors on silicon substrate is quite difficult because of the large lattice mismatch and the crystal structure difference between these materials. To overcome the too large lattice mismatch between III−V or Ge and Si, monolithic integration via oxide buffer layer has been studied since the pioneering work of McKee et al.[4−13] Until now, many experimental[14−17] and theoretical[18−20] investigations have been carried out for the growth of STO on silicon. Recently, the growth of III−V and Ge-based semiconductors on $SrTiO_3$ (STO) buffers becomes more feasible with the progress of growing high-quality crystalline STO on Si substrates;[16,17] and a few works for the growth of GaAs/STO, InP/STO, and Ge/STO have been carried out.[11,12,21,22] However, the growth of III−V or Ge on STO has not been studied thoroughly yet. The initial adsorption processes, atomic structures of semiconductor/oxide interfaces, and growth orientation dependence on the STO surface structures remain not fully understood especially for the situations on STO (001) surfaces that are technologically relevant. Saint-Girons et al. recently observed that the growth orientations of InP and Ge on STO (001) are sensitive to the surface growth conditions.[11,23] The change of semiconductor growth direction from [111] to [001] occurs after annealing STO surface. Unfortunately, detailed knowledge about this dependence is still lacking because of the difficulty to obtain the detailed surface reaction and semiconductor growth information experimentally. First-principles calculation is a tractable method to achieve information for the atom adsorption and layer growth process on surfaces and has been successfully applied to study the atom adsorption and film growth processes on perovskite surfaces.[24−28]

STO(001) has alternating SrO and $TiO_2$ layers; therefore, it can have two nonpolar terminations: SrO and $TiO_2$. The STO(001) 2 × 1 double-layered (DL) $TiO_2$ surface[29,30] adopted in our former[27] and present work is different from other simple $TiO_2$ terminated surfaces, and one of its peculiarities is the occurrence of a floating oxygen atom. This kind of reconstruction was found to be stable in the presence of a substantial amount of oxygen vacancies after annealing the STO surface in UHV before growing semiconductor. In our recent work,[27] we studied the atom adsorption and the route for a (111)-oriented growth of Ge on the STO(001) 2 × 1 $TiO_2$ surface and we successfully compared theoretical results with a soft X-ray photoemission spectroscopy experiment. Our investigation proved that the floating oxygen atom structure is very critical for the Ge(111) growth. However, the surface oxygen atoms will be evaporated and the reconstruction, even if it remains 2 × 1, will be changed after annealing at higher temperature. Recent experimental results show that the dependence of orientation is related to oxygen vacancies.[23] Note that former photoelectron spectroscopy (PES) studies showed that the perovskite surface would become conducting because of the evaporation of surface oxygen atoms.[31,32] Therefore, it is very critical to study the influences of surface oxygen vacancy on the surface reconstruction and following semiconductor thin film growth. In this article, we adopt the

**Received:** February 7, 2013
**Revised:** March 28, 2013
**Published:** April 12, 2013

   dx.doi.org/10.1021/jp4013976 | J. Phys. Chem. C 2013, 117, 9887−9894

epitaxial Ge/STO(001) system as prototypical to study the semiconductor growth orientation dependence on the surface reconstruction conditions. We show that, as opposed to what one could have thought, the reduction of surface (by removing oxygen atoms) favors the creation of the Ge−O bonds by weakening the strength of the Ti−O bonds. By means of calculations of stable configurations during the growth on a reduced surface and the calculation of transition barriers from one to the other, we illustrate the possibility of finding a pathway of a (001) oriented growth.

The article is organized as follows. In section 2, the details of our calculations are described. The main results with particular emphasis on the evolution of surface reconstructions and the dependence of the Ge preferred growth orientation on the reconstructions are respectively presented and discussed in sections 3 and 4. The article closes with a final summary in section 5.

## 2. COMPUTATIONAL DETAILS

In our calculations, we apply the ultrasoft plane-wave pseudopotential density functional method within the generalized gradient approximation (GGA) frameworks as implemented in CASTEP.[33] The Perdew−Burke−Ernzerhof (PBE)[34] version GGA functional provided in CASTEP is adopted here. For the STO and Ge bulk calculations, the Monkhorst−Pack[35] sampling scheme with a k-point mesh of 6 × 6 × 6 in the Brillouin zone is employed. The convergence criteria for energy, force, and displacement of bulk optimizations are respectively $5 \times 10^{-6}$ eV/atom, 0.01 eV/Å, and $5 \times 10^{-4}$ Å. The STO and Ge bulk lattice constant a were calculated to be 3.94 Å and 5.66 Å, respectively. These two values are consistent with other theoretical works and are close to the experimental values, which are 3.90 and 5.65 Å, respectively. Using the calculated lattice parameter, a periodically repeated 11-layer-thick 2 × 1 STO(001) slab-supercell, which is separated from its *z*-direction neighbors by a 20 Å vacuum width, was built and shown in Figure 1.

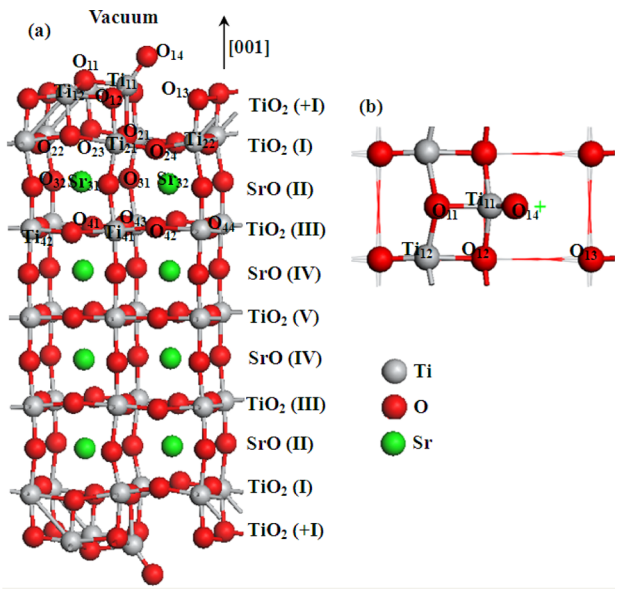


**Figure 1.** Side (a) and top (b) views of STO(001) 2 × 1 $TiO_2$ surface model.

In the slab model surface relaxation and germanium atom adsorption calculations, the computational parameters were different from the bulk lattice parameter computations because of larger computational requirements. Here, the convergence criteria for energy, force, and displacement are respectively $5 \times 10^{-5}$ eV/atom, 0.1 eV/Å, and $5 \times 10^{-3}$ Å. A Monkhorst−Pack sampling scheme with a k-point mesh of 5 × 3 × 1 for surface structure is employed. The plane wave basis set was restricted by a cutoff energy of 380 eV. The adsorption energy per adsorbate atom corresponding to each equilibrium structure is calculated as:

$$\Delta E_{ads} = \frac{E_{total} - E_{slab} - NE_{Ge}}{N} \quad (1)$$

where $N$ is the number of Ge atoms adsorbed on the STO surface. $E_{slab}$, $E_{Ge}$, and $E_{total}$ denote the calculated total energies per supercell calculated for the clean STO slab, isolated Ge atom, and the slab with Ge adsorbed on the surface, respectively. $\Delta E_{ads}$ is negative if the adsorption of atomic Ge on the surface is favorable and exothermic, which is the opposite of the definition of adsorption energy in our previous work[27] to be in agreement with physicist habits. Thus, a lower adsoprtion energy is significant of a more stable configuration.

The transition state searches for oxygen depletion and Ge atom surface diffusion in the present work are performed using synchronous transit methods.[36] Starting from initial and final configurations, the synchronous transit methods can interpolate a reaction pathway to find a transition state. The linear synchronous transit (LST) method performs a single interpolation to a maximum energy. The quadratic synchronous transit (QST) method alternates searches for an energy maximum with constrained minimizations to refine the transition state to a high degree. In present work, we carried out complete LST/QST calculations begin by performing an LST/optimization calculation. QST maximizations will be performed based on the obtained TS approximation. From that point, another conjugate gradient minimization can be performed. This cycle will be repeated until a stationary point is obtained or the limit of set QST steps is reached.

## 3. OXYGEN-DEPLETED $TiO_{2-X}$ SURFACE RECONSTRUCTION

As mentioned earlier, $TiO_2$-terminated surface was found to be stable in the presence of a substantial amount of oxygen vacancies, that is the surface is composed of $TiO_2$ and $TiO_{2-x}$ reconstructions. Therefore, we will first study the structures of $TiO_{2-x}$ surface reconstruction. As shown in Figure 1, the four surface oxygen atoms $O_{11}$, $O_{12}$, $O_{13}$, and $O_{14}$ have different bonding conditions. By removing surface oxygen atom and relaxing, we get three kinds of stable $TiO_{1.5}$ surface structures as shown in Figure 2. Structures 1 and 2 are respectively achieved by removing $O_{11}$ and $O_{13}$ atoms. And removing either $O_{12}$ or $O_{14}$ atoms leads to structure 3. Moreover, the surface O vacancy energies are computed as follows:

$$E_{form}(V_O) = E_{Ti_2O_3} + E_O - E_{Ti_2O_4} \quad (2)$$

$E_{Ti_2O_3}$ and $E_{Ti_2O_4}$ are energies of supercells with and without the vacancy, respectively, and $E_O$ is the oxygen energy in its ground (triplet) state. The surface O vacancy energies of removing $O_{14}$, $O_{13}$, and $O_{11}$ are respectively 4.17, 4.75, and 6.17 eV, which are less than those computed for the F center on the $TiO_2(1 \times 1)$ surface (7.62 eV).[37] By comparing the total energies and O


dx.doi.org/10.1021/jp4013976 | J. Phys. Chem. C 2013, 117, 9887−9894

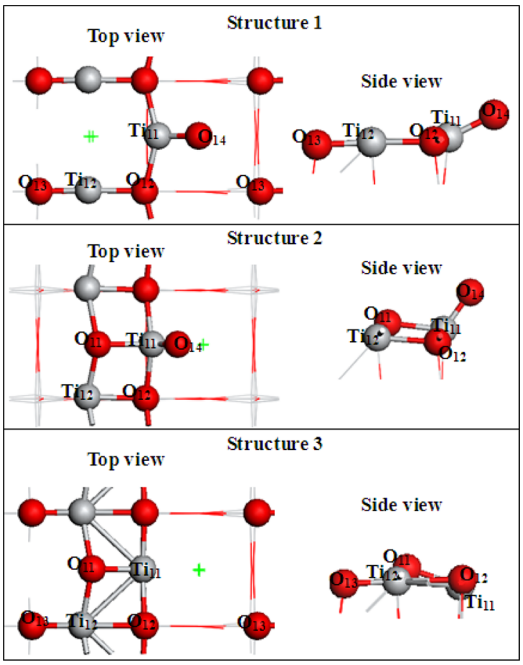


**Figure 2.** Side and top views of three stable STO(001) 2 × 1 $TiO_{1.5}$ surface structures. (a) $O_{11}$ is removed, (b) $O_{13}$ is removed, (c) $O_{12}$ or $O_{14}$ is removed.

vacancy energies of these three structures, we can get that the surface structure 3 is the most stable one.

The energy barriers to remove oxygen atoms from the surface are also calculated by means of the complete LST/QST method.[36] The energy barrier to remove $O_{14}$ is 2.89 eV. However, the energy barrier for removing $O_{11}$ and $O_{13}$ are as high as 8.85 and 7.38 eV, respectively. Therefore, we can get that the structure 3 is the oxygen-depleted $TiO_{1.5}$ surface one which is likely to initially obtain for weak reduction conditions. We thus choose to work on structure 3 knowing that the conclusions obtained will be reinforced for other surfaces.

When we try to further remove surface oxygen atom from the $O_{14}$-depleted $TiO_{1.5}$ surface, higher energy barriers (more than 9 eV) are found. This reflects that TiO surface reconstruction will not be present before all of the $TiO_2$ to $TiO_{1.5}$ transition is finished. Therefore, we can get that $O_{14}$-depleted $TiO_{1.5}$ reconstruction (structure 3 in Figure 2, labeled as $TiO_{1.5}$ in the following context) is the most possible oxygen-depleted $TiO_{2-x}$ surface structure and will be used in the following Ge adsorption investigation.

Let us now study the evolution of the bonding from the bulk to $TiO_2$ and $TiO_{1.5}$ surfaces. For this purpose, we have first computed the Bader[38] partial charges and Mulliken[39] bond populations of surfaces. Bader charge analysis proposed by Bader is based purely on the electronic charge density to obtain the partial atomic charges in molecules. The so-called zero flux surface is used to divide atoms. A zero flux surface is a 2D surface on which the charge density is a minimum perpendicular to the surface. Therefore, Bader charge analysis is basis set independent and has been extensively used in recent years. In present work, our calculations are carried out with plane wave basis functions, which are not associated with any particular atom in the system. Hence, Bader charge analysis is a better choice for the partial atomic charge analysis in present work. However, the Mulliken bonding population analysis is still a useful tool for estimating covalency of bonding and bond strength. Results are respectively shown in Tables 1 and 2. Main assumptions are then illustrated on computed electron density and on local density of states.

**Table 1. Calculated Partial Atomic Charges $Q$ in $|e|$ and Their Deviations from Bulk Values $Q_{bulk}$ ($Q_O$ = −1.26$|e|$, $Q_{Ti}$ = 2.17$|e|$, and $Q_{Sr}$ = 1.60$|e|$) for the Outermost Layers of STO(001) 2 × 1 $TiO_{1.5}$ Surface Compared with Those of 2 × 1 $TiO_2$-Terminated Surface**

| | | $TiO_{1.5}$ | | $TiO_2$[27] | |
|---|---|---|---|---|---|
| layer | atom | $Q$ | $\Delta Q_{bulk}$ | $Q$ | $\Delta Q_{bulk}$ |
| +I | $Ti_{11}$ | 1.79 | −0.38 | 2.02 | −0.15 |
| | $Ti_{12}$ | 1.98 | −0.19 | 2.10 | −0.07 |
| | $O_{11}$ | −1.19 | 0.07 | −1.17 | 0.09 |
| | $O_{12}$ | −1.28 | −0.02 | −1.22 | 0.04 |
| | $O_{13}$ | −0.99 | 0.27 | −0.93 | 0.33 |
| | $O_{14}$ | | | −0.80 | 0.46 |
| I | $Ti_{21}$ | 1.97 | −0.20 | 2.15 | −0.02 |
| | $Ti_{22}$ | 2.15 | 0.02 | 2.17 | 0.00 |
| | $O_{21}$ | −1.21 | 0.05 | −1.22 | 0.04 |
| | $O_{22}$ | −1.15 | 0.11 | −1.18 | 0.08 |
| | $O_{23}$ | −1.17 | 0.09 | −1.15 | 0.11 |
| | $O_{24}$ | −1.16 | 0.10 | −1.15 | 0.11 |
| II | $Sr_{31}$ | 1.61 | 0.01 | 1.61 | 0.01 |
| | $Sr_{32}$ | 1.60 | 0.00 | 1.60 | 0.00 |
| | $O_{31}$ | −1.24 | 0.02 | −1.25 | 0.01 |
| | $O_{32}$ | −1.26 | 0.00 | −1.24 | 0.02 |
| III | $Ti_{41}$ | 2.13 | −0.02 | 2.15 | −0.02 |
| | $Ti_{42}$ | 2.14 | −0.01 | 2.16 | −0.01 |
| | $O_{41}$ | −1.23 | 0.03 | −1.22 | 0.04 |
| | $O_{42}$ | −1.27 | −0.01 | −1.25 | 0.01 |
| | $O_{43}$ | −1.25 | 0.01 | −1.24 | 0.02 |
| | $O_{44}$ | −1.25 | 0.01 | −1.26 | −0.00 |

**Table 2. Calculated Bond Length in Å and Population in $|e|$ the Top Layers of the STO(001) 2 × 1 $TiO_{1.5}$-Terminated Surface**

| | | Length | | Population | |
|---|---|---|---|---|---|
| atom | bond | $TiO_{1.5}$ | $TiO_2$ | $TiO_{1.5}$ | $TiO_2$ |
| $O_{11}$ | $O_{11}$–$Ti_{11}$ | 1.89 | 1.99 | 0.39 | 0.28 |
| | $O_{11}$–$Ti_{12}$ | 2.06 | 2.01 | 0.61 | 0.74 |
| $O_{12}$ | $O_{12}$–$Ti_{11}$ | 1.98 | 2.03 | 0.73 | 0.48 |
| | $O_{12}$–$Ti_{12}$ | 2.31 | 2.13 | 0.08 | 0.18 |
| | $O_{12}$–$Ti_{21}$ | 2.19 | 2.04 | 0.19 | 0.27 |
| $O_{13}$ | $O_{13}$–$Ti_{12}$ | 1.74 | 1.76 | 0.54 | 0.45 |
| | $O_{13}$–$Ti_{22}$ | 2.01 | 1.91 | 0.29 | 0.36 |
| $O_{14}$ | $O_{14}$–$Ti_{11}$ | | 1.62 | | 0.73 |
| $O_{21}$ | $O_{21}$–$Ti_{11}$ | 1.93 | 2.27 | 0.36 | 0.15 |
| $O_{22}$ | $O_{22}$–$Ti_{12}$ | 1.84 | 1.86 | 0.49 | 0.47 |

Former study[27] shows that the Bader partial charges of Ti (2.17$|e|$) and O (−1.26$|e|$) in STO bulk are far from formal ionic charges (4$|e|$ and −2$|e|$) because of the partly covalent nature of the Ti–O bond. The Ti–O bond covalency in $TiO_2$ surface layers is larger than that in the STO bulk because of the larger deviations of surface Ti and O partial charges from formal ionic charges. Looking now at the evolution from $TiO_2$ to $TiO_{1.5}$ surfaces, one may observe that there is a significant decrease of the partial charges ot the topmost Ti atoms. This is due to the removal of the $O_{14}$ atom, which has a strong electronegativity. That means the charge densities around $Ti_{11}$


dx.doi.org/10.1021/jp4013976 | J. Phys. Chem. C 2013, 117, 9887–9894

and $Ti_{12}$ atoms are increased. However, the quantities of negative charges of the three surface oxygen atoms are all increased after reduction. This can be explained by a donation-back-donation mechanism:[40] the surface $Ti_{11}$ atom gains electrons from the collapse of $Ti_{11}-O_{14}$, and successively the neighboring atoms will gain electrons through the back-donation from the $Ti_{11}$ atom. Moreover, from bonding population analysis we can get that the total Ti−O covalency decreases in $TiO_{1.5}$ surface layers. This is accompanied by a global shortening of Ti−O bond lengths.

The density of states (DOS) is the spectrum of the number of energy levels per electronvolt versus energy and can be directly calculated from the energy levels resulting from the calculation of the band structure. Partial (projected) density of states (PDOS) can be plotted for certain angular momenta (e.g., s, p, d, f) on selected atoms. The sum curve of PDOS represents the local density of states (LDOS) when one atom is selected for calculating. The LDOS (illustrated in Figure 3) of

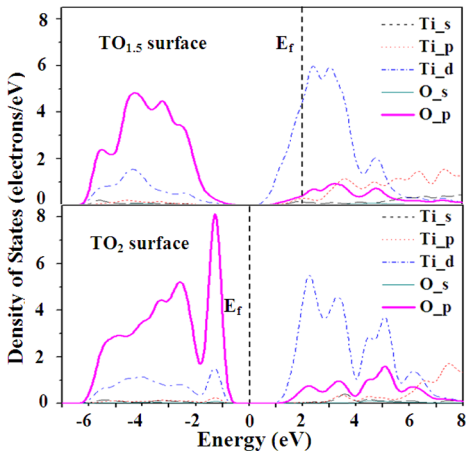


**Figure 3.** Calculated local density of states for $TiO_{1.5}$ and $TiO_2$ surfaces.

$TiO_{1.5}$ and $TiO_2$ surfaces shows that there are strong resonances between Ti and O peaks near the Fermi level. These resonances reflects the Ti−O bonds are formed by mixing Ti 3d orbitals and O 2p orbitals. The electrons of the top of the valence band and the bottom of conduction band are respectively supplied by O 2p and Ti 3d states. For the $TiO_2$ surface, the sharpest peaks at about 0 eV reflect the strongest Ti−O bond (0.73 |e|) between $Ti_{11}$ and $O_{14}$ atoms. However, the narrow peak width of $O_{14}$ 2p compared with the lower 2p peaks (structure from −5 to −1 eV) reflects that the total bonding related to $O_{14}$ is the weakest. This means that the 2p orbitals of $O_{14}$ are far from fully occupied. Therefore, $O_{14}$ atom will be more reactive to adsorbed Ge atoms. For the $TiO_{1.5}$ surface, an about 2 eV Fermi level shift upward into the original conduction-band region with respect to that of the $TiO_2$ surface is observed. PDOS results in Figure 4 show that the removal of $O_{14}$ leads to the decrease of unoccupied 2p orbitals. And the electrons left by the missing O ion are redistributed to the 3d atomic orbitals of the surface Ti atoms, especially on the $Ti_{11}$ ion. This inversion in the type of hydridization of state close to the Fermi level explains the change of reactivity of the STO surface. Therefore, the lower conduction bands are partially occupied, and consequently the surface becomes metallic, as experimentally observed.

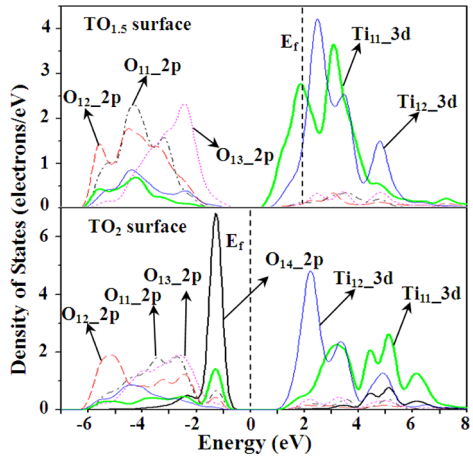


**Figure 4.** Calculated O 2p and Ti 3d partial density of states for $TiO_{1.5}$ and $TiO_2$ surfaces.

## 4. INFLUENCE OF STO SURFACE STRUCTURE ON GE ADSORPTION AND GROWTH

Our research strategy for the simulation of Ge growth on STO is putting Ge atoms one by one on the STO surface to mimic

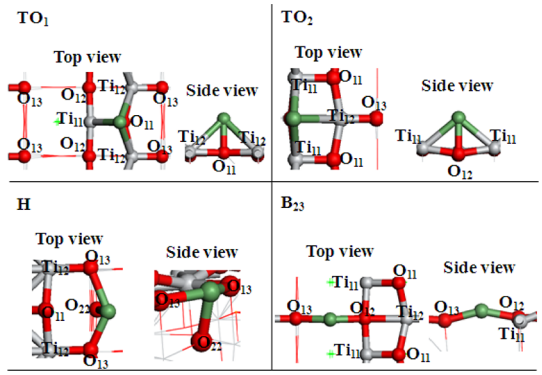


**Figure 5.** Detailed optimized single Ge atom adsorption structures on the $TiO_{1.5}$ surface.

**Table 3. Adsorption Energies of Ge Atom Adsorption on the STO $TiO_{1.5}$ Surface**

| final configuration | adsorption energy (eV/atom) |
|---|---|
| $B_{23}$ | −3.84 |
| H | −3.79 |
| $TO_1$ | −3.50 |
| $TO_2$ | −3.88 |

**Table 4. Migration Energy Barrier (eV) of Ge Adatoms on the STO $TiO_{1.5}$ Surface**

| pathway | forward | reverse |
|---|---|---|
| $B_{23} \rightarrow H$ | 0.45 | 0.40 |
| $B_{23} \rightarrow TO_1$ | 0.36 | 0.02 |
| $B_{23} \rightarrow TO_2$ | 0.43 | 0.47 |
| $H \rightarrow TO_1$ | 0.46 | 0.17 |
| $H \rightarrow TO_2$ | 0.27 | 0.36 |
| $TO_1 \rightarrow TO_2$ | 0.12 | 0.40 |

the early stage of the growth. By calculating the adsorption energies at different sites, we can get the most possible Ge adsorption positions on a surface. With the increasing the


dx.doi.org/10.1021/jp4013976 | J. Phys. Chem. C 2013, 117, 9887−9894

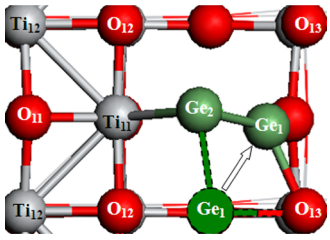


**Figure 6.** Structure transition from $P_2$ to $P_1$.

number of adsorbed Ge atoms, the route for Ge adsorption on the STO surface will be achieved.

Once the structure of the STO (001) $TiO_{1.5}$ surface had been characterized, we proceeded with the adsorption of Ge atoms on it. On the bare $TiO_{1.5}$ surface (shown in Figure 2), there are four kinds of different symmetric adsorption sites: on top of a surface O atom, on top of a surface Ti atom, in the bridge position between two surface O atoms, or in three coordinated sites. We checked the possibilities of all different adsorption sites on the $TiO_{1.5}$ surface. Optimizations of the positions of both the adatom and the atoms at the five surface layers (but keeping the middle layer fixed) are performed to find the equilibrium adsorption geometries. The stable sites of Ge adsorption configurations are labeled and detailed illustrated in Figure 5. These stable configurations can be divided into three groups: (i) On top sites ($TO_1$ and $TO_2$), (ii) 2-fold-coordinated bridge sites ($B_{23}$), and (iii) hollow site H.

Table 3 shows that the lowest adsorption energy corresponds to $TO_{1.5}$ configuration, which is formed by adsorbing Ge on the top of the $O_{12}$ atom. But the energy differences among $TO_2$, $B_{23}$, and H configurations are very small.

By means of the complete LST/QST method,[36] we can find the minimum energy path (MEP) connecting different Ge

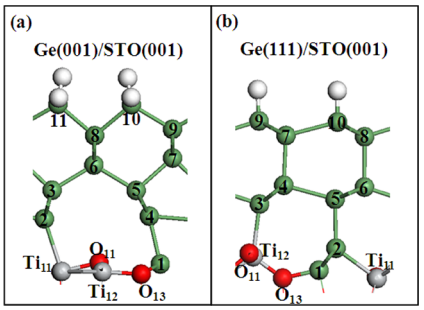


**Figure 8.** Ge(001)/STO(001) (a), and Ge(111)/STO(001) (b) interface structures. All Ge atoms are labeled with their adding sequence. The topmost Ge atoms are saturated with H atoms (white spheres).

adsorption sites and confirmed the energy barriers. Starting from reactants and products, the LST/QST method interpolates a reaction pathway to find a transition state. Our former study shows that $B_{34}$ is the most possible single Ge adsorption configuration on the $TiO_2$ surface by comparing adsorption energies and studying Ge surface migration. However, the Ge migration study on the $TiO_{1.5}$ surface (listed in Table 4) shows that the energy barriers between these four stable sites are similar. This reflects that there is not a most possible single Ge adsorption configuration to act as a nucleation center on the $TiO_{1.5}$ surface. This means we have to be more careful to deal with the following Ge adsorption and growth.

Two different cases are proceeded to consider the adsorption process of a second Ge atom: one where a second Ge atom is introduced on the stable Ge adsorbed surface and another one where two dissociated but closely positioned atoms are placed on the bare surface. After a series of optimizations, the two

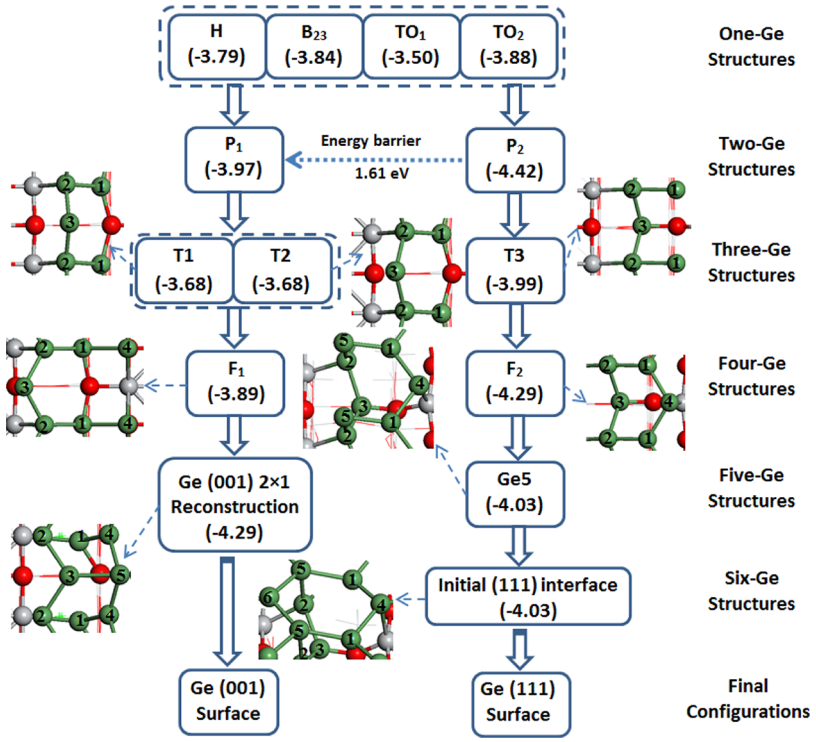


**Figure 7.** Evolutions of the surface structures with the adding of Ge atoms. These numbers in brackets are the corresponding adsorption energy in eV/atom. All Ge atoms are labeled with their adding sequence.


dx.doi.org/10.1021/jp4013976 | J. Phys. Chem. C 2013, 117, 9887−9894

Table 5. Detail Parameters of Ge(001)/STO and Ge(111)/STO Interface Structures Are Compared with Ideal Ge Bulk Bond (2.45 Å) and Angle (109.5°), Ti−Ge Bond Length (2.76 Å),[41] and Ge−O Bond Length in Bulk Germania (1.74 Å)[42]

| interface | parameter | label | value | deviation (%) |
|---|---|---|---|---|
| Ge(001)/STO | bond | $Ge_6$−$Ge_3$ | 2.42 Å | −1.22 |
| | | $Ge_6$−$Ge_5$ | 2.44 Å | −0.41 |
| | | $Ge_6$−$Ge_8$ | 2.41 Å | −1.63 |
| | | $Ge_7$−$Ge_3$ | 2.41 Å | −1.63 |
| | | $Ge_7$−$Ge_5$ | 2.41 Å | −1.63 |
| | | $Ge_7$−$Ge_9$ | 2.40 Å | −2.04 |
| | | $Ge_2$−$Ti_{11}$ | 2.66 Å | −3.62 |
| | | $Ge_1$−$O_{13}$ | 1.94 Å | 10.22 |
| | angle | ∠$Ge_3$−$Ge_6$−$Ge_8$ | 105.4° | −3.74 |
| | | ∠$Ge_3$−$Ge_6$−$Ge_5$ | 121.5° | 10.96 |
| | | ∠$Ge_5$−$Ge_6$−$Ge_8$ | 107.9° | −1.46 |
| | | ∠$Ge_3$−$Ge_7$−$Ge_9$ | 112.0° | 2.28 |
| | | ∠$Ge_5$−$Ge_7$−$Ge_9$ | 111.4° | 1.74 |
| | | ∠$Ge_9$−$Ge_7$−$Ge_9$ | 110.4° | 0.82 |
| Ge(111)/STO | bond | $Ge_4$−$Ge_7$ | 2.44 Å | −0.41 |
| | | $Ge_4$−$Ge_3$ | 2.47 Å | 0.82 |
| | | $Ge_4$−$Ge_5$ | 2.66 Å | 8.57 |
| | | $Ge_6$−$Ge_8$ | 2.47 Å | 0.82 |
| | | $Ge_6$−$Ge_3$ | 2.49 Å | 1.63 |
| | | $Ge_6$−$Ge_5$ | 2.81 Å | 14.69 |
| | | $Ge_7$−$Ge_10$ | 2.71 Å | 10.6 |
| | | $Ge_8$−$Ge_9$ | 2.69 Å | 9.8 |
| | | $Ge_8$−$Ge_10$ | 2.48 Å | 1.2 |
| | | $Ge_2$−$Ti_{11}$ | 2.51 Å | −9.06 |
| | | $Ge_3$−$Ti_{12}$ | 2.59 Å | −5.16 |
| | | $Ge_1$−$O_{13}$ | 1.81 Å | 4.02 |
| | | $Ge_1$−$O_{24}$ | 1.82 Å | 4.60 |
| | angle | ∠$Ge_5$−$Ge_4$−$Ge_3$ | 112.2° | 2.47 |
| | | ∠$Ge_5$−$Ge_4$−$Ge_7$ | 103.1° | −5.84 |
| | | ∠$Ge_3$−$Ge_4$−$Ge_7$ | 112.0° | 2.28 |
| | | ∠$Ge_3$−$Ge_7$−$Ge_9$ | 118.5° | 8.22 |
| | | ∠$Ge_5$−$Ge_7$−$Ge_9$ | 103.2° | −5.75 |
| | | ∠$Ge_9$−$Ge_7$−$Ge_9$ | 107.0° | −2.28 |

most stable Ge atom pair adsorption configurations $P_1$ and $P_2$ are obtained.

The computed values indicate that the transition from $P_1$ to $P_2$ is activated with a low energy cost of about 0.60 eV, whereas the energy barrier (1.61 eV) for the transition from $P_2$ to $P_1$ (illustrated in Figure 6) is about 3 times higher. When transitioning from $P_2$ to $P_1$, only the $Ge_1$ atom needs to migrate. This result reveals that $P_1$ and $P_2$ configurations may coexist at the low growth temperatures. In higher temperature conditions, the high energy barrier from $P_2$ to $P_1$ can be overcome and the existence probability of $P_1$ is increased.

On the basis of these two double Ge atoms' adsorption configurations, we continue to introduce the Ge atom on the $TiO_{1.5}$ surface. Ge (001) and (111) early stage surfaces can be both achieved along two different routes (illustrated in Figure 7) according to the starting configuration. The stable configurations of Ge(001)/STO(001) and Ge(111)/STO(001) interfaces terminated by hydrogen atoms are shown in Figure 8. The STO (001) surface studied in the present work is 2 × 1 reconstruction. Therefore, two Ge atoms can form a Ge monolayer with the periodic boundary condition. In our article, stable and reasonable Ge [001] and [111] direction layers are respectively achieved after 11 and 10 Ge atoms adsorptions (as shown in Figure 8). This means more Ge atoms adding will become the adsorption of Ge atom on Ge (001) or (111) surface, which is beyond the scope of present work.

Let us now detail each route (as illustrated in Figure 7). Starting with configuration $P_2$, a Ge(111)/STO(001) interface is obtained and shown in part b of Figure 8. From the data listed in Table 5, we can get that this interface is also regular. But the computed length of bond $Ge_4$−$Ge_5$ and bond $Ge_6$−$Ge_5$ are respectively is 14.69% and 8.57% larger than ideal value. It looks like the early Ge (111) layer undergoes an important stress inside the first germanium thin layer. We are confident that, even if it represents the most stable interface to obtain a Ge(111) orientation, such epitaxial growth will be difficult to continue on a 2D mode.

Beginning with the pair configuration $P_1$, we supplied further Ge atoms at different sites to investigate the formation of first Ge tetrahedral structure. Our investigation shows that two similar stable structures ($T_1$ and $T_2$ shown in Figure 7) with a 2-fold-coordinated Ge atom are achieved. This point is important for the presence of the Ge (001) surface. Adding more Ge atoms, we can get a structure similar with Ge (001) (shown in part a of Figure 8). This configuration can be regarded as a good foundation for a Ge [001] direction growth. The detailed parameters of the Ge(001)/STO(001) interface are listed in Table 5. Although the bond angles show a little distortion, the Ge−Ge bond lengths listed in Table 5 are well consistent with the that of ideal Ge bulk.

## 5. SUMMARY AND CONCLUSIONS

We have studied in this work the structure of the STO 2 × 1 $TiO_{1.5}$ surface and the Ge adsorption and growth on it by means of systematic first principles calculations. We confirmed the structure of the most stable $TiO_{1.5}$ surface and found that this surface becomes metallic after removing a floating oxygen atom. The redistribution of electrons left by the missing O atom leads to the decrease of surface bonding covalence and the increasing of surface reactivity. Therefore, the following Ge adsorption is affected by this kind of surface structure and electronic changes. By adding Ge atoms one by one on the STO $TiO_{1.5}$ surface, we achieved two growth routes for Ge [001] and [111] directions respectively. Our investigation shows that the STO surface structure and growth temperature are both critical for Ge [001] direction growth. The $TiO_{1.5}$ surface gives the possibility of Ge [001] direction growth. But our calculation shows that [001] direction growth required higher temperature than [111] direction growth. These conclusions occur for the other reduced surfaces as the same kind of electron redistribution surface characteristics will be reinforced.

## AUTHOR INFORMATION

### Corresponding Author

*E-mail: Isabelle.Lefebvre@isen.fr; tel.: (33) 320304028; fax: (33) 320304051.

### Notes

The authors declare no competing financial interest.

## ■ ACKNOWLEDGMENTS

The authors acknowledge financial support from French ANR project COMPHETI, Grant No. ANR-09-NANO-013-01. We also thank Northwestern Polytechnical University High Performance Computing Center for allocation of computing time on their machines.

## ■ REFERENCES

(1) Eisenbeiser, K.; Emrick, R.; Drropad, R.; Yu, Z.; Finder, J.; Rockwell, S.; Holmes, J.; Overgaard, C.; Ooms, W. GaAs MESFETs Fabricated on Si Substrates Using a $SrTiO_3$ Buffer Layer. *IEEE Electron Device Lett.* **2002**, *23*, 300−302.

(2) Seo, J. W.; Dieker, C.; Tapponier, A.; Marchiori, C.; Sousa, M.; Locquet, J.-P.; Fompeyrine, J.; Ipsas, A.; Rossel, C.; Panayiotatos, Y.; Sotiropoulos, A.; Dimoulas, A. Epitaxial Germanium-on-Insulator Grown on (001) Si. *Microelectron. Eng.* **2007**, *84*, 2328−2331.

(3) Saint-Girons, G.; Cheng, J.; Regreny, P.; Largeau, L.; Patriarche, G.; Hollinger, G. Accommodation at the Interface of Highly Dissimilar Semiconductor/Oxide Epitaxial Systems. *Phys. Rev. B* **2009**, *80*, 155308.

(4) McKee, R. A.; Walker, F. J.; Chisholm, M. F. Crystalline Oxides on Silicon: The First Five Monolayers. *Phys. Rev. Lett.* **1998**, *81*, 3014.

(5) Groenert, M. E.; Leitz, C. W.A.; Pitera, J. V.; HarryLee, Y.; Ram, R. J.; Fitzgerald, E. A. Monolithic Integration of Room-Temperature cw GaAs/AlGaAs Lasers on Si Substrates via Relaxed Graded GeSi Buffer Layers. *J. Appl. Phys.* **2003**, *93*, 362−367.

(6) Chriqui, Y.; Saint-Girons, G.; Bouchoule, S.; Isella, G.; VonKaenel, H.; Sagnes, I. Room Temperature Laser Operation of Strained InGaAs/GaAs QW Structure Monolithically Grown by MOVCD on LE-PECVD Ge/Si Virtual Substrate. *Electron. Lett.* **2003**, *39*, 1658−1660.

(7) Forst, C. J.; Schwarz, K.; Blochl, P. E. Structural and Electronic Properties of the Interface between the High-k Oxide $LaAlO_3$ and Si(001). *Phys. Rev. Lett.* **2005**, *95*, 137602.

(8) Bai, J.; Park, J. -S.; Cheng, Z.; Curtin, M.; Adekore, B.; Carroll, M.; Lochtefeld, A.; Dudley, M. Study of the Defect Elimination Mechanisms in Aspect Ratio Trapping Ge Growth. *Appl. Phys. Lett.* **2007**, *90*, 101902.

(9) Saint-Girons, G.; Regreny, P.; Largeau, L.; Patriarche, G.; Hollinger, G. Monolithic Integration of InP based Heterostructures on Silicon Using Crystalline $Gd_2O_3$ Buffers. *Appl. Phys. Lett.* **2007**, *91*, 241912.

(10) Merckling, C.; Delhaye, G.; El-Kazzi, M.; Gaillard, S.; Rozier, Y.; Rapenne, L.; Chenevier, B.; Marty, O.; Saint-Girons, G.; Gendry, M.; Robach, Y.; Hollinger, G. Epitaxial Growth of $LaAlO_3$ on Si(001) Using Interface Engineering. *Microelectron. Reliab.* **2007**, *47*, 540−543.

(11) Cheng, J.; Aviles, T.; El Akra, A.; Bru-Chevallier, C.; Largeau, L.; Patriarche, G.; Regreny, P.; Benamrouche, A.; Robach, Y.; Hollinger, G.; Saint-Girons, G. Optically Active Defects in an InAsP/InP Quantum Well Monolithically Grown on $SrTiO_3$(001). *Appl. Phys. Lett.* **2009**, *95*, 232116.

(12) Cheng, J.; Regreny, P.; Largeau, L.; Patriarche, G.; Mauguin, O.; Naji, K.; Hollinger, G.; Saint-Girons, G. Influence of the Surface Reconstruction on the Growth of InP on $SrTiO_3$(001). *J. Cryst. Growth* **2009**, *311*, 1042−1045.

(13) Giussani, A.; Rodenbach, P.; Zaumseil, P.; Dabrowski, J.; Kurps, R.; Weidner, G.; Schroeder, T. Atomically Smooth and SingleCrystalline Ge(111)/cubic-$Pr_2O_3$(111)/Si(111) Heterostructures: Structural and Chemical Composition Study. *J. Appl. Phys.* **2009**, *105*, 033512.

(14) Tian, H. F.; Yang, H. X.; Zhang, H. R.; Li, Y.; Lu, H. B.; Li, J. Q. Interface of Epitaxial $SrTiO_3$ on Silicon Characterized by Transmission Electron Microscopy, Electron Energy Loss Spectroscopy, and Electron Holography. *Phys. Rev. B* **2006**, *73*, 075325.

(15) Delhaye, G.; Merckling, C.; El-Kazzi, M.; Saint-Girons, G.; Gendry, M.; Robach, Y.; Hollinger, G.; Largeau, L.; Patriarche, G. Structural Properties of Epitaxial $SrTiO_3$ Thin Films Grown by Molecular Beam Epitaxy on Si(001). *J. Appl. Phys.* **2006**, *100*, 124109.

(16) Warusawithana, M. P.; Cen, C.; Sleasman, C. R.; Woicik, J. C.; Li, Y.; Kourkoutis, L. F.; Klug, J. A.; Li, H.; Ryan, P.; Wang, L.-P.; Bedzyk, M.; Muller, D. A.; Chen, L.-Q.; Levy, J.; Schlom, D. G. A Ferroelectric Oxide Made Directly on Silicon. *Science* **2009**, *324*, 367−370.

(17) Niu, G.; Penuelas, J.; Largeau, L.; Vilquin, B.; Maurice, J. L.; Botella, C.; Hollinger, G.; Saint-Girons, G. Evidence for the Formation of Two Phases during the Growth of SrTiO3 on Silicon. *Phys. Rev. B* **2011**, *83*, 054105.

(18) Zhang, X.; Demkov, A. A.; Li, H.; Hu, X.; Wei, Y.; Kulik, J. Atomic and Electronic Structure of the Si/$SrTiO_3$ Interface. *Phys. Rev. B* **2003**, *68*, 125323.

(19) Forst, C. J.; Ashman, C. R.; Schwarz, K.; Blochl, P. E. The Interface between Silicon and a High-k Oxide. *Nature (London)* **2004**, *427*, 53.

(20) Kolpak, A. M.; Ismail-Beigi, S. Thermodynamic Stability and Growth Kinetics of Epitaxial $SrTiO_3$ on Silicon. *Phys. Rev. B* **2011**, *83*, 165318.

(21) Largeau, L.; Patriarche, G.; Saint-Girons, G.; Delhaye, G.; Hollinger, G. Self-assembled Ge Nanocrystals on $BaTiO_3$/$SrTiO_3$/Si(001). *Appl. Phys. Lett.* **2008**, *92*, 031904.

(22) Gobaut, B.; Penuelas, J.; Cheng, J.; Chettaoui, A.; Largeau, L.; Hollinger, G.; Saint-Girons, G. Direct Growth of InAsP/InP Quantum Well Heterostructures on Si Using Crystalline $SrTiO_3$/Si Templates. *Appl. Phys. Lett.* **2010**, *97*, 201908.

(23) El-Kazzi, M.; Gobaut, B.; Penuelas, J.; Grenet, G.; Silly, M.; Sirotti, F.; Saint-Girons, G. Ge/$SrTiO_3$(001) Interface Probed by Soft x-ray Synchrotron-Radiation Time-Resolved Photoemission. *Phys. Rev. B* **2012**, *85*, 075317.

(24) Wei, W.; Dai, Y.; Guo, M.; Yu, L.; Huang, B. Density Functional Characterization of the Electronic Structure and Optical Properties of N-Doped, La-Doped, and N/La-Codoped $SrTiO_3$. *J. Phys. Chem. C* **2009**, *113*, 15046−15050.

(25) Wei, W.; Dai, Y.; Guo, M.; Zhu, Y.; Huang, B. Density Functional Theory Study of Ag Adsorption on $SrTiO_3$ (001) Surface. *J. Phys. Chem. C* **2010**, *114*, 10917−10921.

(26) Adeagbo, W. A.; Fischer, G.; Hergert, W. First-Principles Investigations of Electronic and Magnetic Properties of $SrTiO_3$ (001) Surfaces with Adsorbed Ethanol and Acetone Molecules. *Phys. Rev. B* **2011**, *83*, 195428.

(27) Wang, J.; Lefebvre, I. Germanium Adsorption and Initial Growth on SrTiO3 (001) Surface: A First-Principles Investigation. *J. Phys. Chem. C* **2011**, *115*, 22893−22900.

(28) Cakr, D.; Glseren, O. Adsorption of Pt and Bimetallic PtAu Clusters on the Partially Reduced Rutile (110) $TiO_2$ Surface: A First-Principles Study. *J. Phys. Chem. C* **2012**, *116*, 5735−5746.

(29) Erdman, N.; Poeppelmeier, K. R.; Asta, M.; Warschkow, O.; Ellis, D. E.; Marks, L. D. The Structure and Chemistry of the $TiO_2$-rich Surface of $SrTiO_3$ (001). *Nature* **2002**, *419*, 55−57.

(30) Heifets, E.; Piskunov, S.; Kotomin, E. A.; Zhukovskii, Y. F.; Ellis, D. E. Electronic Structure and Thermodynamic Stability of Double-Layered $SrTiO_3$(001) Surfaces: Ab Initio Simulations. *Phys. Rev. B* **2007**, *75*, 115417.

(31) Nozaki, H.; Satoshi, I. Structural Stability of $BC_2N$. *J. Phys. Chem. Solids* **1996**, *57*, 41−49.

(32) Cai, M. Q.; Zhang, Y. J.; Yin, Z.; Zhang, M. S. First-principles Study of Structural and Electronic Properties of $BaTiO_3$(001) Oxygen-vacancy Surfaces. *Phys. Rev. B* **2005**, *72*, 075406.

(33) Segall, M. D.; Lindan, P. J. D.; Probert, M. J.; Pickard, C. J.; Hasnip, P. J.; Clark, S. J.; Payne, M. C. First-Principles Simulation: Ideas, Illustrations and the CASTEP Code. *J. Phys.: Condens. Matter* **2002**, *14*, 2717−2744.

(34) Perdew, J. P.; Burke, K.; Ernzerhof, M. Generalized Gradient Approximation Made Simple. *Phys. Rev. Lett.* **1996**, *77*, 3865.

(35) Monkhorst, H. J.; Pack, J. D. Special Points for Brillouin-Zone Integrations. *Phys. Rev. B* **1976**, *13*, 5188.

(36) Govind, N.; Petersen, M.; Fitzgerald, G.; King-Smith, D.; Andzelm, J. A Generalized Synchronous Transit Method for Transition State Location. *Comput. Mater. Sci.* **2003**, *28*, 250−258.

(37) Alexandrov, V. E.; Kotomin, E. A.; Maier, J.; Evarestov, R. A. First-Principles Study of Bulk and Surface Oxygen Vacancies in $SrTiO_3$ Crystal. *Eur. Phys. J. B* **2009**, *72*, 53−57.
(38) Bader, R. Atoms in Molecules: A Quantum Theory; Oxford University Press: New York, 1990.
(39) Mulliken, R. S. Electronic Population Analysis on LCAO-MO Molecular Wave Functions. I. *J. Chem. Phys.* **1955**, *23*, 1833−1840.
(40) Wang, C. C.; Zhou, G.; Li, J.; Yan, B. H.; Duan, W. H. Hydrogen-Induced Metallization of Zinc Oxide (21 1 0) Surface and Nanowires: The Effect of Curvature. *Phys. Rev. B* **2008**, *77*, 245303.
(41) Lam, R.; Mar, A. Titanium Germanium Antimonide, TiGeSb. *Acta Crystallogr.* **2009**, *E65*, i68.
(42) Wright, A. C.; Etherington, G.; Desa, J. A. E.; Sinclair, R. N.; Connell, G. A. N.; Mikkelsen, J. C. Neutron Amorphography. *J. Non-Cryst. Solids* **1982**, *49*, 63−102.